

# 000 001 002 003 004 005 006 007 008 009 010 011 012 013 014 015 016 017 018 019 020 021 022 023 024 025 026 027 028 029 030 031 032 033 034 035 036 037 038 039 040 041 042 043 044 045 046 047 048 049 050 051 052 053 PEPGLIDER: ATTRIBUTE REGULARIZED VAE FOR IN- TERPRETABLE AND CONTROLLABLE PEPTIDE DESIGN

Anonymous authors

Paper under double-blind review

## ABSTRACT

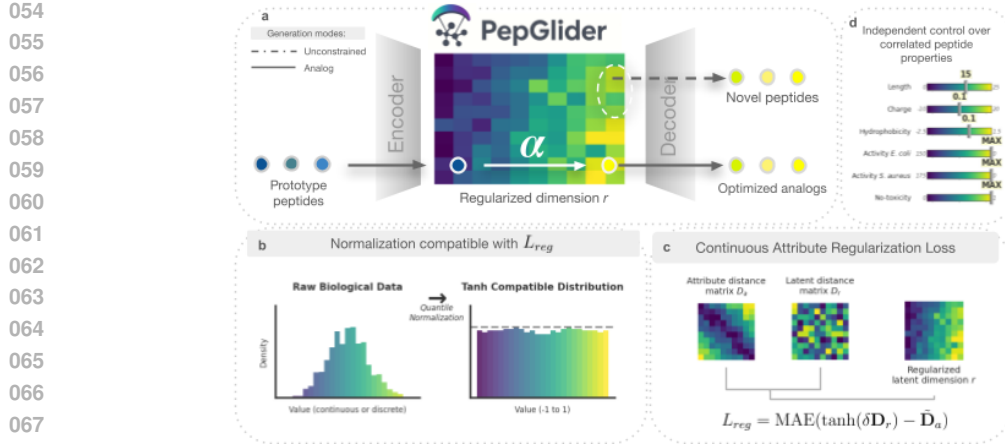
Computational peptide design requires precise control over physicochemical properties that often exhibit complex correlations. Existing generative models rely on simplistic discrete conditioning mechanisms rather than precise targeting of specific property values. We present PepGlider, a continuous attribute regularization framework that enables direct control over specific attribute values. The method achieves structured latent space and displays smooth property gradients with superior disentanglement quality. Experimental results demonstrate that PepGlider enables independent control of naturally correlated properties, and supports both unconstrained generation and targeted optimization of existing peptides. PepGlider applied to antimicrobial peptide design allows generation of candidates with desired antibacterial activity profile. Unlike existing approaches, PepGlider provides precise control over continuous property distributions while maintaining generation quality, offering a generalizable solution for therapeutic and materials applications requiring exact property specifications.

## 1 INTRODUCTION

Peptide design across diverse biomedical applications confronts a fundamental optimization challenge: achieving precise control over continuous peptide properties that often exhibit complex correlations or direct conflicts. Antimicrobial peptide (AMP) design has emerged as particularly urgent due to the escalating antimicrobial resistance crisis. Multidrug-resistant pathogens cause over 700,000 deaths annually, with projections reaching 10 million by 2050 without intervention (O'Neill, 2016). AMPs offer promising alternatives with broad-spectrum activity, rapid bacterial killing kinetics, and reduced resistance development compared to conventional antibiotics (Hancock & Sahl, 2006). The need for controllable peptide design is particularly evident in AMPs, where antimicrobial efficacy depends on complex interplay between physicochemical properties such as charge or hydrophobicity. Introducing positively charged amino acids to increase net charge - crucial for membrane interaction - often disrupts the distribution of hydrophobic residues essential for bacterial killing. Such property interdependencies complicate the optimization of antimicrobial activity, exemplifying the broader challenge of achieving precise control over functional outcomes through correlated molecular characteristics.

Deep generative models have emerged as powerful tools for peptide sequence design, but current approaches exhibit significant limitations in controllability and precision. Existing conditional generation frameworks rely predominantly on discrete conditioning mechanisms that fail to enable precise targeting of specific continuous property values. This limits optimization to coarse-grained categories rather than exact property ranges required for functional applications (Szymczak & Szcurek, 2023). Recent advances in attribute-controllable generation, particularly AR-VAE (Pati & Lerch, 2021), structure latent spaces such that specific dimensions encode target attributes through monotonic relationships. However, AR-VAE's discrete signum-based regularization of the loss function only enable relative ordering between samples, not precise targeting of specific property values. This limitation renders AR-VAE unsuitable for peptide design applications, where achieving functional outcomes requires precise control over exact property ranges.

To address these challenges in controllable peptide design, we present PepGlider, a continuous attribute regularization framework that achieves precise, independent control over correlated peptide properties. Our approach makes three main contributions: (i) we extend AR-VAE with continuous

069 **Figure 1: PepGlider: Continuous attribute regularization for controlled peptide design.**  
070

071 loss formulations that enable precise targeting of specific peptide property values rather than relative  
072 orderings, (ii) we introduce attribute-specific normalization that ensures mathematical compatibility  
073 with continuous loss while preserving biological relevance, particularly adaptive range normalization  
074 for clinically relevant antimicrobial potency ranges, and (iii) we demonstrate independent ma-  
075 nipulation of naturally correlated physicochemical properties through structured latent space design,  
076 enabling multi-objective optimization across conflicting attributes. The resulting framework offers  
077 a generalizable methodology for precise property control across diverse peptide design applications.  
078

## 079 2 METHODS

### 080 2.1 BACKGROUND

083 We build PepGlider upon the Attribute-Regularized VAE framework (Pati & Lerch, 2021), which  
084 structures latent representations such that specific dimensions encode target attributes in a monotonic  
085 fashion. Let  $\mathbf{x}$  denote a data sample (here, a peptide sequence) and  $\mathbf{z}$  represent the corresponding  
086 latent representation obtained through the VAE encoder. For each mini-batch of size  $m$ , the method  
087 constructs attribute and latent distance matrices for all pairs of samples  $i, j \in \{1, \dots, m\}$ :

$$088 \mathbf{D}_a(i, j) = a(\mathbf{x}_i) - a(\mathbf{x}_j) \quad (1)$$

$$089 \mathbf{D}_r(i, j) = z_i^r - z_j^r \quad (2)$$

091 where  $a(\cdot)$  represents the attribute function,  $r$  denotes the regularized latent dimension,  $\mathbf{D}_a$  is the  
092 attribute distance matrix, and  $\mathbf{D}_r$  is the latent distance matrix. The regularization loss enforces  
093 alignment between these distance matrices:

$$095 \mathcal{L}_{\text{attr}} = \text{MAE}(\tanh(\delta \mathbf{D}_r) - \text{sign}(\mathbf{D}_a)) \quad (3)$$

097 The complete AR-VAE objective combines this with standard VAE components:

$$099 \mathcal{L}_{\text{AR-VAE}} = \mathcal{L}_{\text{recon}} + \beta \mathcal{L}_{\text{KL}} + \gamma \sum_{r, a} \mathcal{L}_{\text{attr}}, \quad (4)$$

101 where  $\beta$  controls the weight of the Kullback-Leibler regularization term, while the parameter  $\delta$   
102 controls the spread of latent representations, and  $\gamma$  weights the overall attribute-based regularization  
103 strength.

### 105 2.2 PEPGLIDER FRAMEWORK

107 PepGlider is designed for general peptide design applications requiring precise property control  
across diverse peptide optimization objectives.

108 2.2.1 CONTINUOUS ATTRIBUTE REGULARIZATION  
109110 The discrete nature of the signum function in AR-VAE creates discrete comparisons that limit con-  
111 trollability to relative ordering rather than absolute values. We address this limitation through two  
112 key innovations:113 **Continuous Attribute-Based Regularization** We replace the signum-based comparison with a  
114 continuous regularization formulation. The modified PepGlider loss becomes:

116 
$$\mathcal{L}_{\text{PepGlider}} = \mathcal{L}_{\text{recon}} + \beta \mathcal{L}_{\text{KL}} + \gamma \sum_{r,a} \mathcal{L}_{\text{reg}} \quad (5)$$
  
117

118 where the continuous property regularization term becomes:

120 
$$\mathcal{L}_{\text{reg}} = \text{MAE}(\tanh(\delta \mathbf{D}_r) - \tilde{\mathbf{D}}_a) \quad (6)$$
  
121

122 **Attribute Normalization**  $\tilde{\mathbf{D}}_a$  represents the attribute distance matrix scaled to  $[-1, 1]$ . This for-  
123 mulation enables targeting of specific absolute property values rather than relative comparisons.124 The continuous framework maintains gradient information throughout optimization, enabling fine-  
125 grained control while preserving numerical stability.127 2.2.2 CONTROLLED PEPTIDE GENERATION MODES  
128129 Post-training, PepGlider enables two generation modes that leverage the structured latent space for  
130 different peptide design objectives.132 **Unconstrained generation** samples latent codes  $\mathbf{z} \sim \mathcal{N}(\mathbf{0}, \mathbf{I})$  from the prior distribution and  
133 applies decoder transformations  $\hat{\mathbf{x}} = \text{Dec}(\mathbf{z})$  to produce diverse peptides with desired properties  
134 that reflect the learned distribution of natural sequences. This mode enables exploration of the full  
135 peptide design space without specific property constraints from inputted peptides.137 **Analog generation** enables targeted modification of existing peptides through latent space ma-  
138 nipulation, where a prototype sequence  $\mathbf{x}$  is encoded to  $\mathbf{z} = \text{Enc}(\mathbf{x})$ , modified via  $\alpha$  displacement  
139  $\tilde{\mathbf{z}} = \mathbf{z} + \alpha$  to optimize specific attribute objectives, and reconstructed as  $\hat{\mathbf{x}} = \text{Dec}(\tilde{\mathbf{z}})$ . Here,  $\alpha$   
140 represents the attribute shift vector that directs the latent code toward desired property values in the  
141 structured latent space.142 3 EXPERIMENTAL SETUP  
143

145 Datasets are described in Appendix A.4.

## 147 3.1 ATTRIBUTES

148 **Physicochemical features** PepGlider targets three fundamental physicochemical properties that  
149 serve as key determinants of antimicrobial activity: **net charge** (C, calculated at physiological pH),  
150 **hydrophobicity** (H, average across the sequence), and **sequence length** (L). The selection and com-  
151 putational implementation of these attributes is described in A.4.2.153 **Antimicrobial activity against *E. coli* and *S. aureus*** We incorporate Minimum Inhibitory Con-  
154 centration (MIC) values as continuous attributes predicted by APEX (Wan et al., 2024), a deep learn-  
155 ing model for antimicrobial activity prediction trained on experimentally validated data. We obtain  
156 pathogen-specific MIC predictions for two key bacterial species: MIC against *Escherichia coli* (*E.*  
157 *coli*), averaged over predictions for strains ATCC 11775, AIG222, and AIG221; and MIC against  
158 *Staphylococcus aureus* (*S. aureus*), averaged over ATCC 12600 and ATCC BAA-1556 MRSA.160 **Non-toxicity** To enable safety assessment of generated peptides, we trained a binary classifier to  
161 predict hemolytic toxicity. Hemolytic activity data was extracted from the DBAASP database, focus-  
ing on HC50 measurements (peptide concentration causing 50% hemolysis). Raw toxicity values

underwent rule-based binarization (detailed procedure in A.4.3). Peptide sequences were featurized using a comprehensive set of physicochemical property values, comprising over 100 molecular descriptors including basic properties (length, charge, hydrophobicity), structural descriptors (secondary structure fractions, topological features), and specialized amino acid scales. An XGBoost classifier was trained on these features to predict binary non-toxicity (1 = non-toxic, 0 = toxic).

**Attribute Normalization** We employ quantile normalization (QN) for physicochemical properties and introduce adaptive range normalization for MIC values, providing granular representation of clinically relevant ranges (0-32  $\mu\text{g/ml}$ ) while maintaining the  $[-1, 1]$  scaling required for direct alignment with  $\tanh(\delta D_r)$  outputs. Technical implementation details are in Appendix A.2.1, with data distribution before and after normalization procedure shown in Figure 7.

### 3.2 BASELINES

We evaluate PepGlider against six baseline approaches that represent different paradigms for controlled peptide generation and enable systematic assessment of our methodological contributions. These include ablation variants to isolate the impact of our key innovations (VAE, AR-VAE, PepGlider w/o QN, PepGlider w/ sign, PepGlider w/ z-norm), described in A.4.4, and established VAE-based models for controlled AMP generation (HydrAMP (Szymczak et al., 2023), Transformer-128 (Renaud & Mansbach, 2023)), with detailed descriptions in A.4.5.

### 3.3 EVALUATION METHODOLOGY

Implementation details and training procedure are in Appendix A.4.6. We evaluate our continuous attribute regularization framework across two complementary aspects: fundamental controllability capabilities and domain-specific application. First, we assess core framework capabilities required for controllable peptide design, including latent space disentanglement quality, continuous property control precision, and independent manipulation of correlated physicochemical properties. Second, we demonstrate framework applicability through antimicrobial peptide optimization, showcasing how general controllability enables complex, domain-specific biological objectives. Generated peptides are evaluated using antimicrobial activity predictions, safety assessment, sequence quality metrics (validity, diversity, novelty, antimicrobial potential), and disentanglement quality measures. Detailed evaluation methodology is provided in A.4.7

## 4 RESULTS

### 4.1 DISENTANGLEMENT QUALITY

Effective disentanglement is crucial for controllable generation, as it determines whether individual attributes can be manipulated independently through latent space traversal without unintended side effects on other properties at the same time. Following Pati & Lerch (2021), we assess PepGlider’s disentanglement quality using five established objective metrics: Interpretability, Spearman Correlation Coefficient (SCC), Modularity, Mutual Information Gap (MIG), and Separated Attribute Predictability (SAP) averaged across charge, length, and hydrophobicity (Appendix A.4.7, Table 1).

Model	Interpretability ( $\uparrow$ )	SCC ( $\uparrow$ )	Modularity ( $\uparrow$ )	MIG ( $\uparrow$ )	SAP ( $\uparrow$ )
VAE	0.175	0.389	0.833	0.003	0.023
HydrAMP	0.231	0.487	<b>0.864</b>	0.012	0.025
Transformer-128	0.104	0.365	0.845	0.005	0.039
AR-VAE	0.954	<b>0.995</b>	0.984	0.450	0.741
PepGlider w/ signum	0.955	<b>0.995</b>	0.984	0.453	0.739
PepGlider w/o normalization	<b>0.981</b>	<b>0.995</b>	<b>0.987</b>	<b>0.479</b>	<b>0.771</b>
PepGlider w z-score normalization	0.966	<b>0.995</b>	<b>0.987</b>	0.478	0.753
PepGlider	0.931	<b>0.995</b>	0.985	0.449	0.719

Table 1: **Disentanglement quality metrics for PepGlider and baseline and ablation methods.** Mean scores across three peptide attributes (charge, length, hydrophobicity). Higher scores indicate better disentanglement for all metrics. Attribute-specific results in Table 5.

All AR-VAE variants, including PepGlider, achieve substantially superior disentanglement compared to baseline methods (VAE, HydrAMP, Transformer-128). AR-VAE and its variants demonstrate near-perfect SCC scores ( $\geq 0.995$ ) and high performance across most metrics, with ablation variants occasionally outperforming PepGlider itself. This pattern validates that our modifications preserve the strong disentanglement properties of the original AR-VAE framework while enabling continuous control. The moderate Modularity scores for AR-VAE variants reflect biologically realistic attribute interdependencies in peptide properties, while the dramatic improvements in Interpretability (0.931 vs. 0.231 for best baseline) and MIG (0.449 vs. 0.012) demonstrate effective latent space organization for controllable generation.

#### 4.1.1 CONTINUOUS ATTRIBUTE CONTROL

Practical peptide design requires smooth, predictable property transitions during latent space traversal to enable systematic peptide optimization toward target properties values. We evaluate PepGlider’s continuous control capability using 2D attribute surface plots across regularized latent dimensions and an example, not regularized one. Latent vectors are systematically sampled, decoded, and evaluated for property values.

The resulting surfaces demonstrate smooth, continuous transitions across length, charge, and hydrophobicity (Figure 2, upper panel), enabling precise navigation through the latent space. The quality of latent space traversal is the highest for PepGlider when contrasted with baseline models (Appendix A.5.3). Critically, PepGlider maintains consistently high validity throughout latent space navigation, measured as FBD to training data (A.4.7). Validity assessment across systematic latent shifts (Figure 2, lower panel) shows PepGlider outperforms all baseline models, including VAE, Transformer, and HydrAMP, while AR-VAE variants perform similarly to PepGlider. PepGlider’s consistent validity during traversal ensures that property optimization preserves biological plausibility of generated sequences. Additional amino acid frequency analysis confirms that PepGlider maintains realistic compositional patterns that closely match the training data distribution (Figure 9).

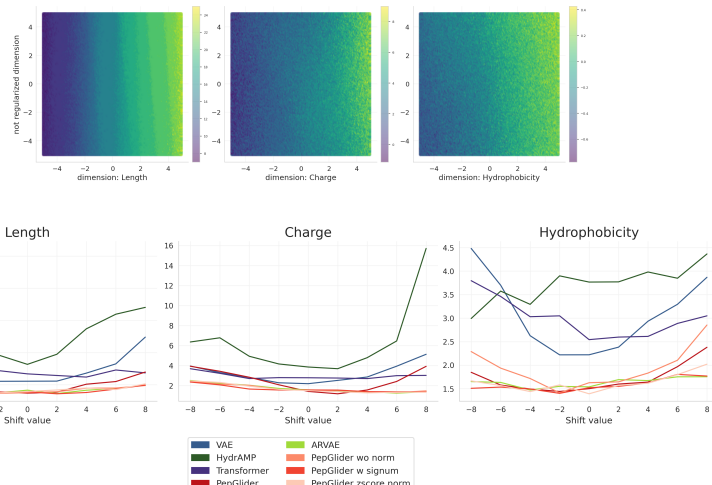


**Figure 2: Continuous attribute control through latent space manipulation.** **Upper panel:** PepGlider 2D attribute surface plots for length, charge, and hydrophobicity showing smooth property transitions. **Lower panel:** Validity (FBD to training data) across latent shifts for PepGlider, baselines, and ablation variants.

#### 4.1.2 INDEPENDENT CONTROL OF CORRELATED PROPERTIES

The ability to manipulate correlated properties addresses conflicting optimization objectives in peptide design. We evaluate PepGlider’s performance in this task through multi-attribute conditioning experiments, constraining different property combinations: individual attributes (L, C, or H), pairs (L+C, L+H, or C+H), or all three simultaneously (L+C+H), measuring target property responses while monitoring cross-interference effects.

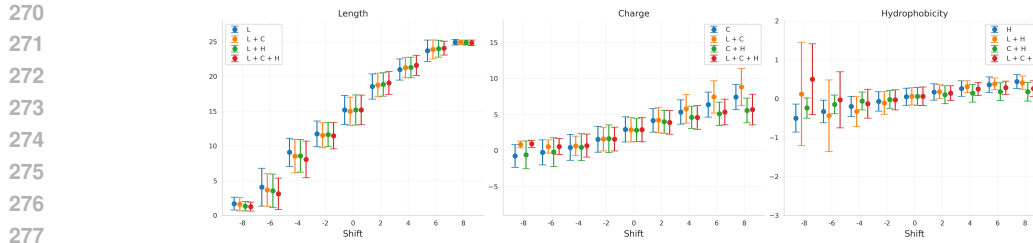


Figure 3: **Independent control of correlated peptide properties through selective attribute conditioning.** Property values across latent space shifts for (a) net charge, (b) sequence length, and (c) hydrophobicity under single-attribute (blue), dual-attribute (orange), and tri-attribute (green) conditioning scenarios. Error bars represent mean  $\pm$  standard deviation.

PepGlider demonstrates precise independent property control across conditioning scenarios (Figure 3). Individual property constraints yield precise linear control over target attributes while leaving non-target properties unchanged. Multi-property conditioning maintains this selective control, with the exception of simultaneous charge and hydrophobicity control (C+H), which shows impairment due to inherent physicochemical constraints where hydrophobic residues are typically uncharged. Non-conflicting combinations (L+C, L+H) achieve precise multi-objective control, where each target property responds predictably to its corresponding latent dimension manipulation.

Comprehensive ablation analysis (Figure 11) reveals PepGlider achieves the greatest range of controllable values across all variants. This expanded dynamic range enables more effective targeting of specific property values and systematic exploration of property regions inaccessible to other approaches, establishing PepGlider’s capability for simultaneous multi-property optimization while maintaining biological realism.

## 4.2 ANTIMICROBIAL ACTIVITY OPTIMIZATION

To demonstrate real-world applicability, we apply our framework to antimicrobial peptide optimization, where complex biological activity must be balanced against multiple physicochemical constraints. While previous sections established continuous control over basic peptide properties, practical utility depends on whether this controllability extends to biological activity predictions. Validity analysis (Figure 12) demonstrates that separating these attribute types enables more stable generation quality across the controllable space, ensuring that complex biological objectives can be pursued without compromising sequence plausibility. Therefore, we proceed with a model trained exclusively on activity and non-toxicity data.

### 4.2.1 ANTIMICROBIAL ACTIVITY CONTROL

To evaluate whether PepGlider’s continuous control extends to complex biological functions, we generate 2D surface plots, where decoded peptides are evaluated using APEX MIC prediction models for *E. coli* and *S. aureus*. The smooth activity gradients across latent space demonstrate systematic control over antimicrobial potency (Figure 4, upper panels). Validation through scatterplot analysis of in-house dataset peptides projected into PepGlider’s latent space reveals that experimentally verified high-activity peptides (low MIC values) naturally cluster in regions associated with predicted antimicrobial efficacy (Figure 4, lower panels), confirming that learned representations capture genuine biological function rather than arbitrary encodings.

### 4.2.2 UNCONSTRAINED GENERATION FOR HIGH-ACTIVITY PEPTIDE DISCOVERY

We evaluate PepGlider’s ability to generate peptides with enhanced antimicrobial activity in the unconstrained generation mode via sampling from high-activity latent regions (see 2.2.2), by comparing its performance against established generative approaches. Two complementary assessments demonstrate both controllability and biological relevance: (1) antimicrobial potential approximated through FBD to active peptides during targeted sampling from high-activity latent regions (Figure 5, upper panel), and (2) direct APEX-predicted MIC distributions for sequences from unconstrained

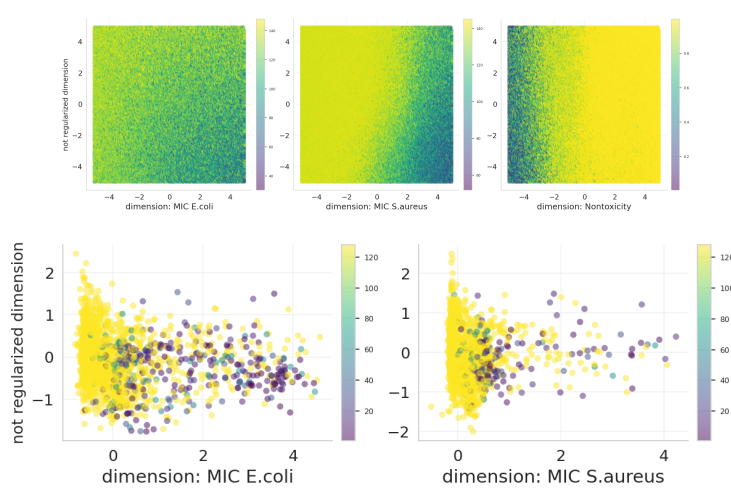


Figure 4: **Continuous antimicrobial activity control in PepGlider latent space.** **Upper panels:** 2D surface plots showing APEX-predicted MIC values across latent space for *E. coli* (left), *S. aureus* (middle), and non-toxicity predictions (right). **Lower panels:** Validation scatterplots showing peptides from proprietary dataset A.4.7 projected into latent space, colored by experimental MIC values for *E. coli* (left) and *S. aureus* (right).

generation (Figure 5, lower panel). Based on Figure 5, we select the best shift combination per strain (+8.0 for *E. coli*, +2.0 for *S. aureus*) and use this setup to calculate sequence metrics, including validity, novelty, and diversity, provided in Table 2.

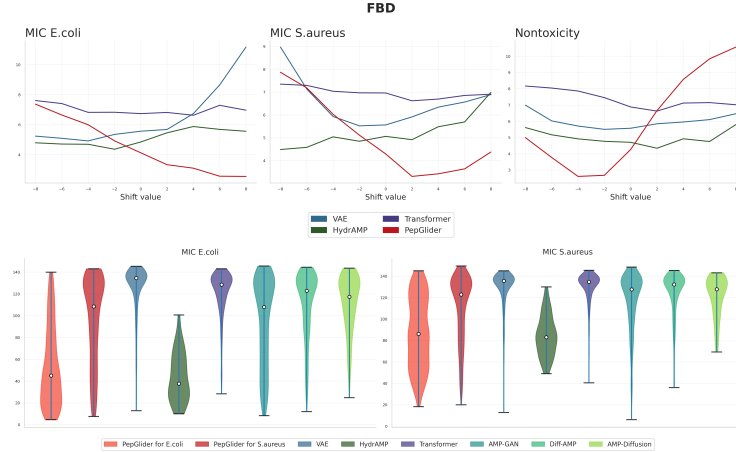
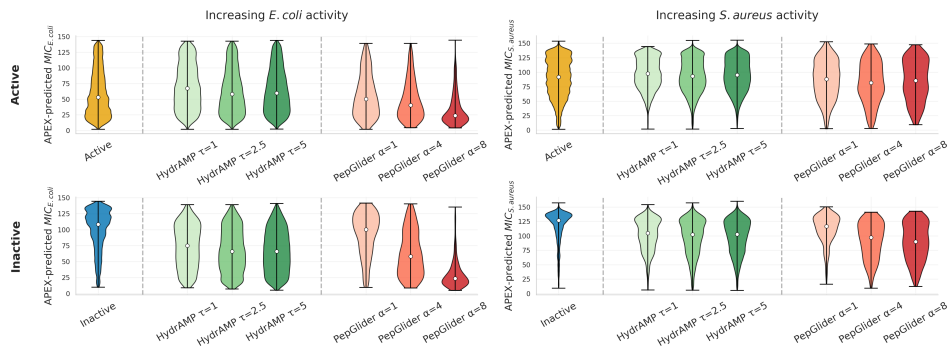


Figure 5: **High-activity peptide generation through strategic latent space sampling.** Fréchet Biological Distance (FBD) scores comparing PepGlider to baseline methods when generating peptides from latent space regions corresponding to low MIC predictions. FBD computed between generated samples and reference set of highly active antimicrobial peptides using fine-tuned ESM2 embeddings. Lower FBD scores indicate greater similarity to genuine high-activity antimicrobial peptides.

The results demonstrate PepGlider’s superior performance in unconstrained generation of high-activity antimicrobial candidates. APEX predictions (Figure 5, lower panel) show that PepGlider-generated sequences achieve substantially lower MIC distributions for both *E. coli* and *S. aureus* compared to all baseline and external methods. For *E. coli*, PepGlider’s unconstrained generation produces a concentrated distribution around 40-60  $\mu\text{g}/\text{ml}$  with significant density below 32  $\mu\text{g}/\text{ml}$  (clinically relevant threshold), while competing methods show broader distributions centered at higher MIC values. Similarly, for *S. aureus*, PepGlider maintains low MIC predictions with

378  
379  
380  
381  
382  
383

Model	Validity (↓)	AMP potential (↓)	Novelty (↑)	Diversity (↑)
VAE	2.201	5.671	1.0	0.988
HydrAMP	3.616	4.950	1.0	0.897
Transformer	2.668	6.827	1.0	<b>1.144</b>
AMP-GAN	2.202	5.705	1.0	0.990
Diff-AMP	3.237	4.254	1.0	0.940
AMP <sub>Diffusion</sub>	3.936	8.036	1.0	0.825
PepGlider*	<b>1.498</b>	<b>2.935</b>	1.0	0.956

384  
385  
386  
387  
Table 2: **Sequence quality metrics for unconstrained generation across generative models.**  
Comparison of validity, AMP potential, novelty, and diversity for PepGlider and baseline/external  
generative methods. \*PepGlider results averaged over *E. coli* and *S. aureus* predictions.388  
389  
390  
391  
392  
393  
394  
395  
396  
397  
398  
399400  
401  
402  
403  
Figure 6: **Existing peptide improvement through analog generation.** Violin plots showing anti-  
404  
405  
406  
407  
408  
409  
410  
411  
412  
413  
414  
415  
416  
417  
418  
419  
420  
421  
422  
423  
424  
425  
426  
427  
428  
429  
430  
431  
432  
433  
434  
435  
436  
437  
438  
439  
440  
441  
442  
443  
444  
445  
446  
447  
448  
449  
450  
451  
452  
453  
454  
455  
456  
457  
458  
459  
460  
461  
462  
463  
464  
465  
466  
467  
468  
469  
470  
471  
472  
473  
474  
475  
476  
477  
478  
479  
480  
481  
482  
483  
484  
485  
486  
487  
488  
489  
490  
491  
492  
493  
494  
495  
496  
497  
498  
499  
500  
501  
502  
503  
504  
505  
506  
507  
508  
509  
510  
511  
512  
513  
514  
515  
516  
517  
518  
519  
520  
521  
522  
523  
524  
525  
526  
527  
528  
529  
530  
531  
532  
533  
534  
535  
536  
537  
538  
539  
540  
541  
542  
543  
544  
545  
546  
547  
548  
549  
550  
551  
552  
553  
554  
555  
556  
557  
558  
559  
560  
561  
562  
563  
564  
565  
566  
567  
568  
569  
570  
571  
572  
573  
574  
575  
576  
577  
578  
579  
580  
581  
582  
583  
584  
585  
586  
587  
588  
589  
590  
591  
592  
593  
594  
595  
596  
597  
598  
599  
600  
601  
602  
603  
604  
605  
606  
607  
608  
609  
610  
611  
612  
613  
614  
615  
616  
617  
618  
619  
620  
621  
622  
623  
624  
625  
626  
627  
628  
629  
630  
631  
632  
633  
634  
635  
636  
637  
638  
639  
640  
641  
642  
643  
644  
645  
646  
647  
648  
649  
650  
651  
652  
653  
654  
655  
656  
657  
658  
659  
660  
661  
662  
663  
664  
665  
666  
667  
668  
669  
670  
671  
672  
673  
674  
675  
676  
677  
678  
679  
680  
681  
682  
683  
684  
685  
686  
687  
688  
689  
690  
691  
692  
693  
694  
695  
696  
697  
698  
699  
700  
701  
702  
703  
704  
705  
706  
707  
708  
709  
710  
711  
712  
713  
714  
715  
716  
717  
718  
719  
720  
721  
722  
723  
724  
725  
726  
727  
728  
729  
730  
731  
732  
733  
734  
735  
736  
737  
738  
739  
740  
741  
742  
743  
744  
745  
746  
747  
748  
749  
750  
751  
752  
753  
754  
755  
756  
757  
758  
759  
750  
751  
752  
753  
754  
755  
756  
757  
758  
759  
760  
761  
762  
763  
764  
765  
766  
767  
768  
769  
770  
771  
772  
773  
774  
775  
776  
777  
778  
779  
770  
771  
772  
773  
774  
775  
776  
777  
778  
779  
780  
781  
782  
783  
784  
785  
786  
787  
788  
789  
780  
781  
782  
783  
784  
785  
786  
787  
788  
789  
790  
791  
792  
793  
794  
795  
796  
797  
798  
799  
790  
791  
792  
793  
794  
795  
796  
797  
798  
799  
800  
801  
802  
803  
804  
805  
806  
807  
808  
809  
800  
801  
802  
803  
804  
805  
806  
807  
808  
809  
810  
811  
812  
813  
814  
815  
816  
817  
818  
819  
810  
811  
812  
813  
814  
815  
816  
817  
818  
819  
820  
821  
822  
823  
824  
825  
826  
827  
828  
829  
820  
821  
822  
823  
824  
825  
826  
827  
828  
829  
830  
831  
832  
833  
834  
835  
836  
837  
838  
839  
830  
831  
832  
833  
834  
835  
836  
837  
838  
839  
840  
841  
842  
843  
844  
845  
846  
847  
848  
849  
840  
841  
842  
843  
844  
845  
846  
847  
848  
849  
850  
851  
852  
853  
854  
855  
856  
857  
858  
859  
850  
851  
852  
853  
854  
855  
856  
857  
858  
859  
860  
861  
862  
863  
864  
865  
866  
867  
868  
869  
860  
861  
862  
863  
864  
865  
866  
867  
868  
869  
870  
871  
872  
873  
874  
875  
876  
877  
878  
879  
870  
871  
872  
873  
874  
875  
876  
877  
878  
879  
880  
881  
882  
883  
884  
885  
886  
887  
888  
889  
880  
881  
882  
883  
884  
885  
886  
887  
888  
889  
890  
891  
892  
893  
894  
895  
896  
897  
898  
899  
890  
891  
892  
893  
894  
895  
896  
897  
898  
899  
900  
901  
902  
903  
904  
905  
906  
907  
908  
909  
900  
901  
902  
903  
904  
905  
906  
907  
908  
909  
910  
911  
912  
913  
914  
915  
916  
917  
918  
919  
910  
911  
912  
913  
914  
915  
916  
917  
918  
919  
920  
921  
922  
923  
924  
925  
926  
927  
928  
929  
920  
921  
922  
923  
924  
925  
926  
927  
928  
929  
930  
931  
932  
933  
934  
935  
936  
937  
938  
939  
930  
931  
932  
933  
934  
935  
936  
937  
938  
939  
940  
941  
942  
943  
944  
945  
946  
947  
948  
949  
940  
941  
942  
943  
944  
945  
946  
947  
948  
949  
950  
951  
952  
953  
954  
955  
956  
957  
958  
959  
950  
951  
952  
953  
954  
955  
956  
957  
958  
959  
960  
961  
962  
963  
964  
965  
966  
967  
968  
969  
960  
961  
962  
963  
964  
965  
966  
967  
968  
969  
970  
971  
972  
973  
974  
975  
976  
977  
978  
979  
970  
971  
972  
973  
974  
975  
976  
977  
978  
979  
980  
981  
982  
983  
984  
985  
986  
987  
988  
989  
980  
981  
982  
983  
984  
985  
986  
987  
988  
989  
990  
991  
992  
993  
994  
995  
996  
997  
998  
999  
990  
991  
992  
993  
994  
995  
996  
997  
998  
999  
1000  
1001  
1002  
1003  
1004  
1005  
1006  
1007  
1008  
1009  
1000  
1001  
1002  
1003  
1004  
1005  
1006  
1007  
1008  
1009  
1010  
1011  
1012  
1013  
1014  
1015  
1016  
1017  
1018  
1019  
1010  
1011  
1012  
1013  
1014  
1015  
1016  
1017  
1018  
1019  
1020  
1021  
1022  
1023  
1024  
1025  
1026  
1027  
1028  
1029  
1020  
1021  
1022  
1023  
1024  
1025  
1026  
1027  
1028  
1029  
1030  
1031  
1032  
1033  
1034  
1035  
1036  
1037  
1038  
1039  
1030  
1031  
1032  
1033  
1034  
1035  
1036  
1037  
1038  
1039  
1040  
1041  
1042  
1043  
1044  
1045  
1046  
1047  
1048  
1049  
1040  
1041  
1042  
1043  
1044  
1045  
1046  
1047  
1048  
1049  
1050  
1051  
1052  
1053  
1054  
1055  
1056  
1057  
1058  
1059  
1050  
1051  
1052  
1053  
1054  
1055  
1056  
1057  
1058  
1059  
1060  
1061  
1062  
1063  
1064  
1065  
1066  
1067  
1068  
1069  
1060  
1061  
1062  
1063  
1064  
1065  
1066  
1067  
1068  
1069  
1070  
1071  
1072  
1073  
1074  
1075  
1076  
1077  
1078  
1079  
1070  
1071  
1072  
1073  
1074  
1075  
1076  
1077  
1078  
1079  
1080  
1081  
1082  
1083  
1084  
1085  
1086  
1087  
1088  
1089  
1080  
1081  
1082  
1083  
1084  
1085  
1086  
1087  
1088  
1089  
1090  
1091  
1092  
1093  
1094  
1095  
1096  
1097  
1098  
1099  
1090  
1091  
1092  
1093  
1094  
1095  
1096  
1097  
1098  
1099  
1100  
1101  
1102  
1103  
1104  
1105  
1106  
1107  
1108  
1109  
1100  
1101  
1102  
1103  
1104  
1105  
1106  
1107  
1108  
1109  
1110  
1111  
1112  
1113  
1114  
1115  
1116  
1117  
1118  
1119  
1110  
1111  
1112  
1113  
1114  
1115  
1116  
1117  
1118  
1119  
1120  
1121  
1122  
1123  
1124  
1125  
1126  
1127  
1128  
1129  
1120  
1121  
1122  
1123  
1124  
1125  
1126  
1127  
1128  
1129  
1130  
1131  
1132  
1133  
1134  
1135  
1136  
1137  
1138  
1139  
1130  
1131  
1132  
1133  
1134  
1135  
1136  
1137  
1138  
1139  
1140  
1141  
1142  
1143  
1144  
1145  
1146  
1147  
1148  
1149  
1140  
1141  
1142  
1143  
1144  
1145  
1146  
1147  
1148  
1149  
1150  
1151  
1152  
1153  
1154  
1155  
1156  
1157  
1158  
1159  
1150  
1151  
1152  
1153  
1154  
1155  
1156  
1157  
1158  
1159  
1160  
1161  
1162  
1163  
1164  
1165  
1166  
1167  
1168  
1169  
1160  
1161  
1162  
1163  
1164  
1165  
1166  
1167  
1168  
1169  
1170  
1171  
1172  
1173  
1174  
1175  
1176  
1177  
1178  
1179  
1170  
1171  
1172  
1173  
1174  
1175  
1176  
1177  
1178  
1179  
1180  
1181  
1182  
1183  
1184  
1185  
1186  
1187  
1188  
1189  
1180  
1181  
1182  
1183  
1184  
1185  
1186  
1187  
1188  
1189  
1190  
1191  
1192  
1193  
1194  
1195  
1196  
1197  
1198  
1199  
1190  
1191  
1192  
1193  
1194  
1195  
1196  
1197  
1198  
1199  
1200  
1201  
1202  
1203  
1204  
1205  
1206  
1207  
1208  
1209  
1200  
1201  
1202  
1203  
1204  
1205  
1206  
1207  
1208  
1209  
1210  
1211  
1212  
1213  
1214  
1215  
1216  
1217  
1218  
1219  
1210  
1211  
1212  
1213  
1214  
1215  
1216  
1217  
1218  
1219  
1220  
1221  
1222  
1223  
1224  
1225  
1226  
1227  
1228  
1229  
1220  
1221  
1222  
1223  
1224  
1225  
1226  
1227  
1228  
1229  
1230  
1231  
1232  
1233  
1234  
1235  
1236  
1237  
1238  
1239  
1230  
1231  
1232  
1233  
1234  
1235  
1236  
1237  
1238  
1239  
1240  
1241  
1242  
1243  
1244  
1245  
1246  
1247  
1248  
1249  
1240  
1241  
1242  
1243  
1244  
1245  
1246  
1247  
1248  
1249  
1250  
1251  
1252  
1253  
1254  
1255  
1256  
1257  
1258  
1259  
1250  
1251  
1252  
1253  
1254  
1255  
1256  
1257  
1258  
1259  
1260  
1261  
1262  
1263  
1264  
1265  
1266  
1267  
1268  
1269  
1260  
1261  
1262  
1263  
1264  
1265  
1266  
1267  
1268  
1269  
1270  
1271  
1272  
1273  
1274  
1275  
1276  
1277  
1278  
1279  
1270  
1271  
1272  
1273  
1274  
1275  
1276  
1277  
1278  
1279  
1280  
1281  
1282  
1283  
1284  
1285  
1286  
1287  
1288  
1289  
1280  
1281  
1282  
1283  
1284  
1285  
1286  
1287  
1288  
1289  
1290  
1291  
1292  
1293  
1294  
1295  
1296  
1297  
1298  
1299  
1290  
1291  
1292  
1293  
1294  
1295  
1296  
1297  
1298  
1299  
1300  
1301  
1302  
1303  
1304  
1305  
1306  
1307  
1308  
1309  
1300  
1301  
1302  
1303  
1304  
1305  
1306  
1307  
1308  
1309  
1310  
1311  
1312  
1313  
1314  
1315  
1316  
1317  
1318  
1319  
1310  
1311  
1312  
1313  
1314  
1315  
1316  
1317  
1318  
1319  
1320  
1321  
1322  
1323  
1324  
1325  
1326  
1327  
1328  
1329  
1320  
1321  
1322  
1323  
1324  
1325  
1326  
1327  
1328  
1329  
1330  
1331  
1332  
1333  
1334  
1335  
1336  
1337  
1338  
1339  
1330  
1331  
1332  
1333  
1334  
1335  
1336  
1337  
1338  
1339  
1340  
1341  
1342  
1343  
1344  
1345  
1346  
1347  
1348  
1349  
1340  
1341  
1342  
1343  
1344  
1345  
1346  
1347  
1348  
1349  
1350  
1351  
1352  
1353  
1354  
1355  
1356  
1357  
1358  
1359  
1350  
1351  
1352  
1353  
1354  
1355  
1356  
1357  
1358  
1359  
1360  
1361  
1362  
1363  
1364  
1365  
1366  
1367  
1368  
1369  
1360  
1361  
1362  
1363  
1364  
1365  
1366  
1367  
1368  
1369  
1370  
1371  
1372  
1373  
1374  
1375  
1376  
1377  
1378  
1379  
1370  
1371  
1372  
1373  
1374  
1375  
1376  
1377  
1378  
1379  
1380  
1381  
1382  
1383  
1384  
1385  
1386  
1387  
1388  
1389  
1380  
1381  
1382  
1383  
1384  
1385  
1386  
1387  
1388  
1389  
1390  
1391  
1392  
1393  
1394  
1395  
1396  
1397  
1398  
1399  
1390  
1391  
1392  
1393  
1394  
1395  
1396  
1397  
1398  
1399  
1400  
1401  
1402  
1403  
1404  
1405  
1406  
1407  
1408  
1409  
1400  
1401  
1402  
1403  
1404  
1405  
1406  
1407  
1408  
1409  
1410  
1411  
1412  
1413  
1414  
1415  
1416  
1417  
1418  
1419  
1410  
1411  
1412  
1413  
1414  
1415  
1416  
1417  
1418  
1419  
1420  
1421  
1422  
1423  
1424  
1425  
1426  
1427  
1428  
1429  
1420  
1421  
1422  
1423  
1424  
1425  
1426  
1427  
1428  
1429  
1430  
1431  
1432  
1433  
1434  
1435  
1436  
1437  
1438  
1439  
1430  
1431  
1432  
1433  
1434  
1435  
1436  
1437  
1438  
1439  
1440  
1441  
1442  
1443  
1444  
1445  
1446  
1447  
1448  
1449  
1440  
1441  
1442  
1443  
1444  
1445  
1446  
1447  
1448  
1449  
1450  
1451  
1452  
1453  
1454  
1455  
1456  
1457  
1458  
1459  
1450  
1451  
1452  
1453  
1454  
1455  
1456  
1457  
1458  
1459  
1460  
1461  
1462  
1463  
1464  
1465  
1466  
1467  
1468  
1469  
1460  
1461  
1462  
1463  
1464  
1465  
1466  
1467  
1468  
1469  
1470  
1471  
1472  
1473  
1474  
1475  
1476  
1477  
1478  
1479  
1470  
1471  
1472  
1473  
1474  
1475  
1476  
1477  
1478  
1479  
1480  
1481  
1482  
1483  
1484  
1485  
1486  
1487  
1488  
1489  
1480  
1481  
1482  
1483  
1484  
1485  
1486  
1487  
1488  
1489  
1490  
1491  
1492  
1493  
1494  
1495  
1496  
1497  
1498  
1499  
149

432 this trade-off through simultaneous manipulation of MIC and non-toxicity regularized dimensions.  
 433 While manipulating MIC-regularized dimensions to enhance antimicrobial activity against *E. coli*  
 434 and *S. aureus*, we simultaneously apply different non-toxicity regularization strategies ( $\alpha = -2, 0,$   
 435  $+2$  for non-toxicity regularized dimension, as well as random control) to assess whether toxicity  
 436 increases can be mitigated.

437 The results (Figure 13) demonstrate PepGlider’s capacity for controlled multi-objective optimization.  
 438 As expected, shifting toward lower MIC values in the regularized dimensions successfully  
 439 enhances predicted antimicrobial activity for both bacterial targets. Critically, simultaneous non-  
 440 toxicity regularization ( $\alpha = +2$ ) helps maintain higher non-toxicity scores compared to unregularized  
 441 approaches, demonstrating that PepGlider can partially decouple the activity-safety trade-off. This  
 442 capability enables rational optimization of therapeutic windows, allowing researchers to enhance  
 443 antimicrobial potency while minimizing safety risks.

444

## 445 5 DISCUSSION

446

447 PepGlider addresses fundamental limitations in controllable peptide design through continuous  
 448 attribute regularization and adaptive normalization strategies. Our framework enables indepen-  
 449 dent manipulation of correlated properties while maintaining biological plausibility, demonstrated  
 450 through superior latent quality evaluation and systematic property control across challenging sce-  
 451 narios like activity-safety trade-offs.

452

453 Key limitations include reduced performance for inherently conflicting objectives, particularly the  
 454 activity-safety trade-off where enhanced antimicrobial potency often correlates with increased tox-  
 455 icticity. Future developments should prioritize methods that efficiently utilize sparse biological ex-  
 456 perimental data directly, reducing dependence on intermediate prediction models while maintaining  
 457 controllability. The current attribute set, while comprehensive for basic physicochemical properties,  
 458 could be expanded to include synthesizability constraints, structural features (secondary structure  
 459 propensity, flexibility), and manufacturing considerations critical for therapeutic translation.

460

461 The continuous attribute regularization framework’s versatility extends beyond antimicrobial pep-  
 462 tides to diverse therapeutic applications, providing a flexible framework for controllable generation.

463

## 464 6 ETHICS STATEMENT

465

466 This research involves computational design of antimicrobial peptides using machine learning meth-  
 467 ods. All datasets used for training and evaluation consist of publicly available peptide sequences  
 468 and experimental measurements from established databases (AMPScanner, dbAMP, DRAMP,  
 469 DBAASP). No human subjects, animal experiments, or clinical trials were involved in this com-  
 470 putational study. The potential therapeutic applications of designed antimicrobial peptides could  
 471 contribute to addressing antimicrobial resistance, a significant global health challenge. However,  
 472 any peptides generated by this framework require extensive experimental validation, safety testing,  
 473 and regulatory approval before clinical consideration. The hemolytic toxicity predictions used in  
 474 this work are computational estimates and cannot replace experimental safety assessment.

475

476

## 477 7 REPRODUCIBILITY STATEMENT

478

479 We provide comprehensive implementation details to ensure reproducibility. Model architectures,  
 480 hyperparameters, and training procedures are detailed in the main text and appendix (Table 3). All  
 481 normalization procedures, including quantile transformation and adaptive range normalization, are  
 482 mathematically specified with explicit equations. Evaluation metrics and baseline comparisons use  
 483 established methods with clear mathematical definitions. The proprietary validation dataset con-  
 484 tains experimental MIC measurements that enable independent performance assessment, though  
 485 specific data cannot be shared due to proprietary restrictions. Code and trained models will be made  
 486 available upon publication to facilitate reproduction and extension of this work. The framework’s  
 487 implementation using standard deep learning libraries ensures compatibility with common research  
 488 environments.

486 8 LLM USAGE  
487488 Large language models were used as writing assistance tools during the preparation of this  
489 manuscript. Specifically, Claude was employed for improving clarity and flow of technical expla-  
490 nitions, and generating alternative phrasings for complex methodological concepts, proofreading and  
491 copy-editing assistance.492 All scientific content, experimental design, results, and conclusions are entirely the work of the  
493 human authors. LLMs were not used for experimental design decisions, or scientific reasoning. The  
494 core contributions, methodological innovations, and technical implementations represent original  
495 research by the authors. All factual claims and experimental results were verified independently by  
496 the research team.  
497498 REFERENCES  
499500 Yuri Burda, Roger Grosse, and Ruslan Salakhutdinov. Importance weighted autoencoders. *arXiv*  
501 *preprint arXiv:1509.00519*, 2015.502 Payel Das, Tom Sercu, Kahini Wadhawan, Inkit Padhi, Sebastian Gehrmann, Flaviu Cipcigan, Vijil  
503 Chenthamarakshan, Hendrik Strobelt, Cicero Dos Santos, Pin-Yu Chen, et al. Accelerated an-  
504 timicrobial discovery via deep generative models and molecular dynamics simulations. *Nature*  
505 *Biomedical Engineering*, 5(6):613–623, 2021.506  
507 Xiaojie Guo, Yuanqi Du, and Liang Zhao. Property controllable variational autoencoder via invert-  
508 ible mutual dependence. In *International Conference on Learning Representations*, 2020.509  
510 Robert EW Hancock and Hans-Georg Sahl. Antimicrobial and host-defense peptides as new anti-  
511 infective therapeutic strategies. *Nature biotechnology*, 24(12):1551–1557, 2006.512 Martin Heusel, Hubert Ramsauer, Thomas Unterthiner, Bernhard Nessler, and Sepp Hochreiter.  
513 Gans trained by a two time-scale update rule converge to a local nash equilibrium. *Advances in*  
514 *neural information processing systems*, 30, 2017.515  
516 Irina Higgins, Loic Matthey, Arka Pal, Christopher Burgess, Xavier Glorot, Matthew Botvinick,  
517 Shakir Mohamed, and Alexander Lerchner. beta-vae: Learning basic visual concepts with a  
518 constrained variational framework. In *International conference on learning representations*, 2017.519  
520 Xinyue Kang, Fanyi Dong, Cheng Shi, Shicai Liu, Jian Sun, Jiaxin Chen, Haiqi Li, Hanmei Xu,  
521 Xingzhen Lao, and Heng Zheng. Dramp 2.0, an updated data repository of antimicrobial peptides.  
522 *Scientific data*, 6(1):148, 2019.523  
524 Diederik P Kingma and Max Welling. Auto-encoding variational bayes. *arXiv preprint*  
525 *arXiv:1312.6114*, 2013.526  
527 Jack Klys, Jake Snell, and Richard Zemel. Learning latent subspaces in variational autoencoders.  
528 *Advances in neural information processing systems*, 31, 2018.529  
530 Zeming Lin, Halil Akin, Roshan Rao, Brian Hie, Zhongkai Zhu, Wenting Lu, Nikita Smetanin,  
531 Robert Verkuil, Ori Kabeli, Yaniv Shmueli, et al. Evolutionary-scale prediction of atomic-level  
532 protein structure with a language model. *Science*, 379(6637):1123–1130, 2023.533  
534 Alex T Müller, Gisela Gabernet, Jan A Hiss, and Gisbert Schneider. modlamp: Python for antimicro-  
535 bial peptides. *Bioinformatics*, 33(17):2753–2755, 2017.536  
537 Jim O'Neill. Tackling drug-resistant infections globally: final report and recommendations. *The*  
538 *Review on Antimicrobial Resistance*, 2016.539  
540 Amir Pandi, David Adam, Amir Zare, Van Tuan Trinh, Stefan L Schaefer, Marie Burt, Björn  
541 Klabunde, Elizaveta Bobkova, Manish Kushwaha, Yeganeh Foroughijabbari, et al. Cell-free  
542 biosynthesis combined with deep learning accelerates de novo-development of antimicrobial pep-  
543 tides. *Nature Communications*, 14(1):7197, 2023.

540 Ashis Pati and Alexander Lerch. Attribute-based regularization of latent spaces for variational auto-  
 541 encoders. *Neural Computing and Applications*, 33(9):4429–4444, 2021.  
 542

543 Malak Pirtskhalava, Anthony A Armstrong, Maia Grigolava, Mindia Chubinidze, Evgenia Alim-  
 544 barashvili, Boris Vishnepolsky, Andrei Gabrielian, Alex Rosenthal, Darrell E Hurt, and Michael  
 545 Tartakovsky. Dbaasp v3: database of antimicrobial/cytotoxic activity and structure of peptides  
 546 as a resource for development of new therapeutics. *Nucleic acids research*, 49(D1):D288–D297,  
 547 2021.

548 Samuel Renaud and Rachael A Mansbach. Latent spaces for antimicrobial peptide design. *Digital  
 549 Discovery*, 2(2):441–458, 2023.  
 550

551 Yechiel Shai and Ziv Oren. From “carpet” mechanism to de-novo designed diastereomeric cell-  
 552 selective antimicrobial peptides. *Peptides*, 22(10):1629–1641, 2001.

553 Paulina Szymczak and Ewa Szczurek. Artificial intelligence-driven antimicrobial peptide discovery.  
 554 *Current Opinion in Structural Biology*, 83:102733, 2023.  
 555

556 Paulina Szymczak, Marcin Mozejko, Tomasz Grzegorzek, Radoslaw Jurczak, Marta Bauer, Damian  
 557 Neubauer, Karol Sikora, Michal Michalski, Jacek Sroka, Piotr Setny, et al. Discovering highly  
 558 potent antimicrobial peptides with deep generative model hydram. *nature communications*, 14  
 559 (1):1453, 2023.

560 Sophia Tang, Yinuo Zhang, and Pranam Chatterjee. Peptune: De novo generation of therapeutic  
 561 peptides with multi-objective-guided discrete diffusion. *ArXiv*, pp. arXiv–2412, 2025.  
 562

563 Marcelo DT Torres, Leo Tianlai Chen, Fangping Wan, Pranam Chatterjee, and Cesar de la Fuente-  
 564 Nunez. Generative latent diffusion language modeling yields anti-infective synthetic peptides.  
 565 *Cell Biomaterials*, 2025.

566 Colin M Van Oort, Jonathon B Ferrell, Jacob M Remington, Safwan Wshah, and Jianing Li. Ampgan  
 567 v2: machine learning-guided design of antimicrobial peptides. *Journal of chemical information  
 568 and modeling*, 61(5):2198–2207, 2021.

569 Daniel Veltri, Uday Kamath, and Amarda Shehu. Deep learning improves antimicrobial peptide  
 570 recognition. *Bioinformatics*, 34(16):2740–2747, 2018.  
 571

572 Fangping Wan, Marcelo DT Torres, Jacqueline Peng, and Cesar de la Fuente-Nunez. Deep-learning-  
 573 enabled antibiotic discovery through molecular de-extinction. *Nature Biomedical Engineering*, 8  
 574 (7):854–871, 2024.  
 575

576 Rui Wang, Tao Wang, Linlin Zhuo, Jinhang Wei, Xiangzheng Fu, Quan Zou, and Xiaojun Yao. Diff-  
 577 amp: tailored designed antimicrobial peptide framework with all-in-one generation, identification,  
 578 prediction and optimization. *Briefings in Bioinformatics*, 25(2), 2024.

579 Shiyu Wang, Xiaojie Guo, Xuanyang Lin, Bo Pan, Yuanqi Du, Yinkai Wang, Yanfang Ye, Ashley  
 580 Petersen, Austin Leitgeb, Saleh AlKhalifa, et al. Multi-objective deep data generation with cor-  
 581 related property control. *Advances in neural information processing systems*, 35:28889–28901,  
 582 2022.

583 Torsten Weprecht, Margitta Dathe, Eberhard Krause, Michael Beyermann, W Lee Maloy,  
 584 Dorothy L MacDonald, and Michael Bienert. Modulation of membrane activity of amphipathic,  
 585 antibacterial peptides by slight modifications of the hydrophobic moment. *FEBS letters*, 417(1):  
 586 135–140, 1997.  
 587

588 Lantian Yao, Jiahui Guan, Peilin Xie, Chia-Ru Chung, Zhihao Zhao, Danhong Dong, Yilin Guo,  
 589 Wenyang Zhang, Junyang Deng, Yuxuan Pang, et al. dbamp 3.0: updated resource of antimicro-  
 590 bial activity and structural annotation of peptides in the post-pandemic era. *Nucleic acids  
 591 research*, 53(D1):D364–D376, 2025.

592 Michael R Yeaman and Nannette Y Yount. Mechanisms of antimicrobial peptide action and resis-  
 593 tance. *Pharmacological reviews*, 55(1):27–55, 2003.

594 **A APPENDIX**  
595596 **A.1 RELATED WORK**  
597598 Controllable peptide design intersects multiple research areas, including conditional generation and  
599 latent space regularization, each addressing different aspects of the challenge of navigating corre-  
600 lated peptide properties.601 **Controllable Peptide Design** Current approaches to controllable peptide generation, particularly  
602 for AMPs, employ three main strategies: conditional generation, post-hoc filtering, and guidance  
603 during sampling. While conditional methods like HydrAMP (Szymczak et al., 2023) directly in-  
604 incorporate constraints, they are limited to binary classification or struggle with multiple objectives.  
605 Post-hoc approaches (Das et al., 2021; Pandi et al., 2023; Torres et al., 2025) suffer from severe  
606 efficiency limitations when targeting rare property combinations. The exponential search space of  
607 peptide sequences makes exhaustive sampling impractical, particularly when multiple properties  
608 must be optimized simultaneously. Guidance-based methods attempt to steer the generation process  
609 toward desired properties during sampling, including approaches that use Monte Carlo Tree Guid-  
610 ance (Tang et al., 2025) and reinforcement learning with property-based rewards (Wang et al., 2024).  
611 However, guidance approaches operate at the sampling level rather than embedding controllability  
612 into the learned representation, making them computationally expensive during generation and un-  
613 able to leverage the structured relationships between properties for more efficient optimization.614 **Latent Space Regularization** Latent space regularization methods from other domains learn rep-  
615 resentations where properties naturally align with latent structure. VAE-based approaches have  
616 pioneered this direction through various regularization strategies. CorrVAE (Wang et al., 2022) ad-  
617 dresses property correlations through specialized loss functions designed to handle interdependent  
618 data characteristics. Property-controllable VAE (Guo et al., 2020) incorporates property predic-  
619 tion losses directly into the variational objective, creating latent representations that encode desired  
620 features. Conditional Subspace VAE (Klys et al., 2018) partitions the latent space according to  
621 property-specific regions, enabling targeted sampling from relevant subspaces. AR-VAE (Pati &  
622 Lerch, 2021) aligns latent and attribute spaces through distance matrix matching to create mono-  
623 tonic relationships between latent dimensions and target properties. While these latent space meth-  
624 ods offer promising frameworks for controllable generation, they have not been adapted to address  
625 the specific challenges of peptide design, particularly the need for precise property targeting across  
626 correlated physicochemical characteristics and efficient access to rare, but functional attribute com-  
627 binations essential for therapeutic applications.628 **A.2 EXTENDED METHODS**  
629630 **A.2.1 ATTRIBUTE NORMALIZATION PROCEDURES**  
631632 We introduce attribute-specific normalization strategies as a core methodological contribution that  
633 ensures compatibility with our continuous loss formulation while preserving biological meaning.634 **Quantile Normalization** Applied to charge, length, hydrophobicity, and non-toxicity predictions.  
635 Raw values are transformed via quantile transformation  $Q(\cdot)$  to uniform distribution  $U(0, 1)$ , then  
636 linearly scaled:

637 
$$\tilde{p}_i = 2Q(p_i) - 1 \tag{7}$$

638 This ensures uniform property space coverage and eliminates scale bias while maintaining the re-  
639 quired  $[-1, 1]$  range.640 **Adaptive Range Normalization** A normalization strategy that addresses the clinical importance of  
641 low MIC values while maintaining loss compatibility. The approach allocates 70% of the normalized  
642 range to therapeutically relevant concentrations (0-32  $\mu\text{g/ml}$ ) and 30% to higher values:643 *Higher concentrations ( $>32 \mu\text{g/ml}$ )  $\rightarrow [-1, -0.4]$ :*

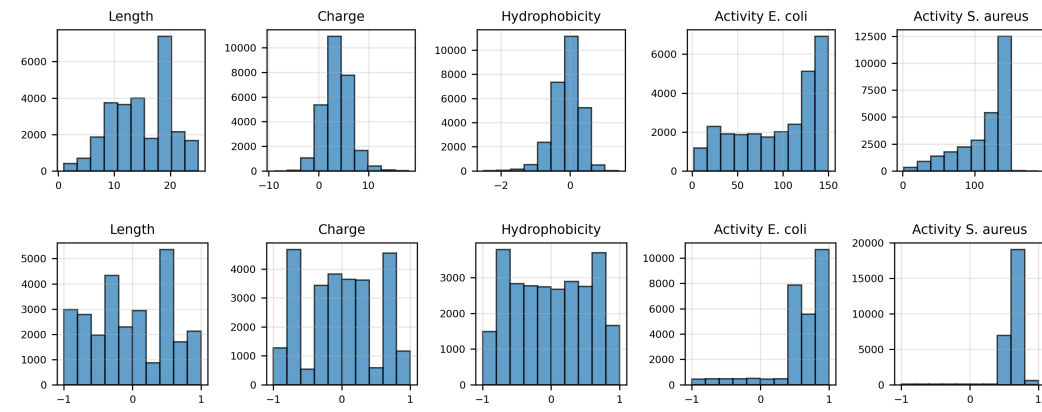
644 
$$\tilde{p}_{out} = -1 + 0.6 \cdot \text{CDF}_{out}(p) \tag{8}$$

645 *Clinically relevant range (0-32  $\mu\text{g/ml}$ )  $\rightarrow [-0.4, 1]$ :*

646 
$$\tilde{p}_{ROI} = -0.4 + 1.4 \cdot \text{CDF}_{ROI}(p) \tag{9}$$

648 where  $CDF_{ROI}$  and  $CDF_{out}$  are empirical cumulative distribution functions computed within each  
 649 region using histogram-based quantile mapping.  
 650

651 This normalization framework enables precise property control by ensuring all normalized attributes  
 652 operate within the same bounded range as the latent regularization terms. Unlike the discrete ap-  
 653 proach that rely on signum function, our continuous formulation maintains gradient information  
 654 throughout optimization, enabling fine-grained control over peptide properties while preserving  
 655 compatibility with standard VAE training procedures.  
 656



657  
 658  
 659  
 660  
 661  
 662  
 663  
 664  
 665  
 666  
 667  
 668  
 669  
 670  
 671  
 672 **Figure 7: Two-stage normalization procedure for continuous attribute regularization.** Distribu-  
 673 tion comparison of peptide properties before (upper panel) and after (lower panel) the normaliza-  
 674 tion procedure.  
 675  
 676

### A.3 EXTENDED EXPERIMENTAL SETUP

### A.4 DATASETS

680 The training dataset comprises 27331 curated antimicrobial peptide sequences derived from  
 681 four comprehensive databases: AMPScanner (Veltri et al., 2018), dbAMP (Yao et al., 2025),  
 682 DRAMP (Kang et al., 2019), and DBAASP (Pirtskhala et al., 2021). Sequences are restricted  
 683 to a maximum of 25 amino acid residues, capturing the predominant length range of naturally oc-  
 684 ccurring antimicrobial peptides. Duplicate sequences are removed across databases to ensure unique  
 685 representation within the training corpus.  
 686

#### A.4.1 EVALUATION DATASET

687 For evaluation of PepGlider, we utilize a proprietary dataset containing experimental MIC measure-  
 688 ments for 1,736 peptides tested against 11 clinically relevant bacterial strains. The dataset includes  
 689 measurements against Gram-negative bacteria (*A. baumannii* ATCC 19606, *E. coli* ATCC 11775,  
 690 *E. coli* AIC221, carbapenem-resistant *E. coli* AIC222, *K. pneumoniae* ATCC 13883, *P. aeruginosa*  
 691 PAO1 and PA14) and Gram-positive bacteria (*S. aureus* ATCC 12600, methicillin-resistant *S. au-*  
 692 *reus* ATCC BAA-1556, vancomycin-resistant *E. faecalis* ATCC 700802, and vancomycin-resistant  
 693 *E. faecium* ATCC 700221). This comprehensive dataset enables validation of generated peptides  
 694 against both standard reference strains and clinically significant drug-resistant isolates, providing  
 695 robust assessment of antimicrobial activity across diverse bacterial targets.  
 696

#### A.4.2 PHYSICOCHEMICAL PROPERTIES

697 We selected net charge, hydrophobicity, and sequence length as target attributes for PepGlider based  
 698 on their established roles in antimicrobial peptide function and their ability to discriminate between  
 699 active and inactive peptides.  
 700

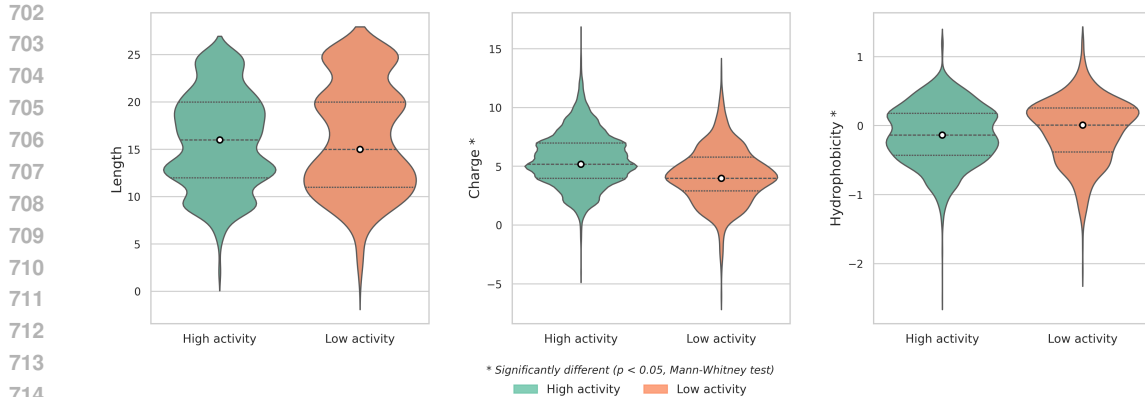


Figure 8: **Discriminative physicochemical properties between active and inactive antimicrobial peptides.** Distribution comparison of net charge, hydrophobicity, and sequence length between active peptides (green) and inactive peptides (orange) from the curated dataset.

**Net Charge** plays a critical role in the initial electrostatic interactions between cationic antimicrobial peptides and negatively charged bacterial membranes (Yeaman & Yount, 2003). Positively charged residues facilitate binding to bacterial lipopolysaccharides and phospholipids, while excessive charge can lead to reduced membrane permeation and potential cytotoxicity (Hancock & Sahl, 2006). Net charge is calculated at physiological pH (7.0), accounting for the ionization state of terminal groups and ionizable side chains based on their respective pKa values from the *modlamp* implementation.

**Hydrophobicity** determines the peptide’s ability to partition into and disrupt bacterial membranes (Wieprecht et al., 1997). Optimal hydrophobic content enables membrane insertion while preventing aggregation or excessive hemolytic activity. Average hydrophobicity is computed using established amino acid hydrophobicity scales:

$$H(\mathbf{x}) = \frac{1}{L} \sum_{i=1}^L h_i \quad (10)$$

where  $h_i$  represents the hydrophobicity value for amino acid  $i$  and  $L$  is the sequence length.

**Sequence length** constrains both structural flexibility and membrane interaction mechanisms. Shorter peptides typically adopt extended conformations that facilitate membrane carpet formation, while longer sequences may form more complex secondary structures affecting activity and selectivity (Shai & Oren, 2001). Sequence length is a direct enumeration of amino acid residues:

$$L(\mathbf{x}) = |\mathbf{x}| \quad (11)$$

Physicochemical properties are computed using the *modlamp* (Müller et al., 2017) package, implementing algorithms for antimicrobial peptide analysis:

To validate these properties as discriminative features, we analyzed their distributions across active ( $\text{MIC} \leq 32 \mu\text{g/ml}$ ) and inactive ( $\text{MIC} \geq 128 \mu\text{g/ml}$ ) peptides in our curated dataset (Figure 8). Active peptides exhibit distinct distributions for all three properties: moderate positive charge (mean  $\pm$  SD), intermediate hydrophobicity values, and concentrated length distributions around 10–25 residues. These clear distributional differences support their selection as target attributes for continuous control in the PepGlider framework.

#### A.4.3 NON-TOXICITY

**Data Extraction and Preprocessing** Hemolytic activity measurements were extracted from DBAASP (Pirtskhala et al., 2021), focusing on records containing HC50 values and percentage

756 hemolysis data. Activity measure values and groups were normalized to lowercase for consistent  
 757 processing. Percentage hemolysis values were extracted using regex parsing with two prioritized  
 758 patterns: (1) values with standard deviations (e.g., “15.2±3.1% hemolysis”), taking the primary  
 759 value before  $\pm$ , and (2) range formats (e.g., “10-20% hemolysis”), using the midpoint average.  
 760

761 **Binary Toxicity Classification Rules** For peptides with single measurements, the following hier-  
 762 archy was applied:

- 763 • Direct non-toxic assignment: 0% hemolysis records  $\rightarrow$  non-toxic (1)
- 764 • Activity-based toxic assignment: activity  $\leq 32 \mu\text{g/mL}$  AND  $> 1\%$  hemolysis  $\rightarrow$  toxic (0)
- 765 • Activity-based non-toxic assignment: activity  $> 32 \mu\text{g/mL}$  AND  $\leq 10\%$  hemolysis  $\rightarrow$  non-  
 766 toxic (1)
- 767 • Hemolysis threshold:  $> 50\%$  hemolysis  $\rightarrow$  toxic (0)
- 768 • HC50-specific rules:  $\text{HC50} \leq 256 \mu\text{g/mL} \rightarrow$  toxic (0), otherwise non-toxic (1)

771 For peptides with multiple measurements, consensus rules were applied:

- 772 • Any measurement  $< 32 \mu\text{g/mL} \rightarrow$  toxic (0)
- 773 • All measurements  $> 128 \mu\text{g/mL} \rightarrow$  non-toxic (1)
- 774 • All measurements  $\leq 10\%$  hemolysis  $\rightarrow$  evaluate based on activity ( $< 32 \mu\text{g/mL}$  threshold  
 775 for toxic (0))
- 776 • HC50 measurements prioritized when available, using  $128 \mu\text{g/mL}$  threshold (toxic (0) if  
 777  $\leq 128 \mu\text{g/mL}$ )

780 Peptides not meeting any classification criteria were excluded from the training dataset.

781 **Feature Engineering** The physicochemical property calculation framework computed 100+ fea-  
 782 tures per sequence, including:

- 783 • Basic properties: length, charge, isoelectric point, molecular weight, aromaticity
- 784 • Hydrophobicity scales: AASI, Argos, Eisenberg, GRAVY, Kyte-Doolittle (16 scales total)
- 785 • Structural descriptors: secondary structure fractions, flexibility, entropy
- 786 • Specialized scales: Z-scales (5D), Kidera factors (10D), VHSE scales (8D), FASGAI vec-  
 787 tors (6D)
- 788 • Topological features: polar surface area, H-bond acceptors/donors, rotatable bonds
- 789 • Compositional features: amino acid frequencies, structural class distributions

790 **Model Training and Validation** XGBoost classifier hyperparameters were optimized on the train-  
 791 ing set with 974,582 peptides (1,157 toxic and 973,425 non-toxic) balanced using focal loss set to  
 792 handle the imbalanced dataset. Model performance was assessed on the independent HydrAMP  
 793 dataset containing experimentally validated antimicrobial peptides with known hemolytic profiles  
 (Accuracy = 0.8333, F1-Score = 0.9048).

#### 794 A.4.4 ABLATIONS

801 **VAE Baseline** serves as our primary ablation control, employing the identical transformer-based  
 802 VAE architecture as PepGlider with Importance Weighted Autoencoder components and  $\beta$ -VAE  
 803 regularization. The model is trained on the same dataset with identical quantile normalization,  
 804 but without the continuous attribute regularization loss ( $\gamma = 0$ ) and and 10-times decreased  $\beta$ .  
 805 This configuration isolates the contribution of our continuous regularization framework from the  
 806 architectural and preprocessing components.

807 **AR-VAE** (Pati & Lerch, 2021) represents the original attribute regularization formulation using the  
 808 signum function for discrete ordinal comparisons and standard preprocessing without quantile nor-  
 809 malization. This baseline evaluates the impact of our continuous loss formulation and normalization  
 improvements.

810 **PepGlider w/o QN** removes quantile normalization while retaining the continuous loss formulation  
 811 and signum replacement. Raw attribute values are used directly in the loss computation, isolating  
 812 the contribution of the normalization procedure.

813 **PepGlider w/ sign** retains the original signum function from AR-VAE while incorporating our quan-  
 814 tile normalization approach. This variant evaluates whether normalization alone can improve dis-  
 815 crete attribute regularization.

816 **PepGlider w/ z-norm** replaces quantile normalization with standard z-score normalization (zero  
 817 mean, unit variance), testing alternative normalization strategies while maintaining the continuous  
 818 loss formulation.

#### 820 A.4.5 BASELINE MODELS

821 **HydrAMP** (Szymczak et al., 2023) is a conditional variational autoencoder for antimicrobial peptide  
 822 generation. The model employs Jacobian-based disentanglement regularization to enforce indepen-  
 823 dence between latent representations  $\mathbf{z}$  and discrete conditioning variables ( $c_{AMP}, c_{MIC} \in \{0, 1\}$ ).  
 824 Property control is achieved through conditional decoding  $\text{Dec}(\mathbf{z}, c)$  with binary labels for anti-  
 825 microbial activity and potency. In contrast to PepGlider’s continuous attribute regularization in latent  
 826 space, HydrAMP guides generation through discrete conditions fed directly to the decoder. The  
 827 model supports unconstrained generation and temperature-controlled analogue generation modes.

828 **Transformer-128** (Renaud & Mansbach, 2023) employs a transformer-based autoencoder architec-  
 829 ture with a 128-dimensional latent space for peptide generation. The model learns implicit parti-  
 830 tioning of the latent space into regions corresponding to high and low AMP probabilities without  
 831 explicit incorporation of mechanisms for continuous property control.

#### 832 A.4.6 PEPGLIDER IMPLEMENTATION

833 PepGlider employs a transformer-based VAE architecture (Kingma & Welling, 2013) optimized  
 834 for variable-length biological sequences. The encoder  $\text{Enc}(\cdot)$  maps peptide sequences  $\mathbf{x} \in$   
 835  $\{A, C, D, \dots, Y\}^L$  to latent representations  $\mathbf{z} \in \mathbb{R}^d$  through CLS token aggregation, where a learn-  
 836 able classification token attends to all sequence positions via multi-head self-attention mechanisms.  
 837 The encoder outputs parameterize a Gaussian posterior  $q(\mathbf{z}|\mathbf{x})$  with mean  $\mu(\mathbf{x})$  and standard devi-  
 838 ation  $\sigma(\mathbf{x})$ . The decoder  $\text{Dec}(\cdot)$  reconstructs sequences from latent codes by replicating the latent  
 839 vector across sequence positions and applying positional encodings for position-specific token  
 840 generation. The architecture incorporates  $\beta$ -VAE regularization (Higgins et al., 2017) and Importance  
 841 Weighted Autoencoder components (Burda et al., 2015) to enhance posterior distribution approxi-  
 842 mation and latent space disentanglement capabilities.

843 All models were trained on NVIDIA A100 GPUs with 8GB memory. PepGlider and baseline models  
 844 were trained for approximately 48 hours. The hyperparameter details are presented in Table 3.

845 **Training Schedule:** The  $\beta$  and  $\gamma$  parameter follow linear annealing schedules from their initial to  
 846 final values over the specified warmup steps, after which they remain constant. The KL divergence  
 847 weight  $\beta$  gradually increases to prevent posterior collapse.

#### 848 A.4.7 EVALUATION METHODOLOGY

849 **Antimicrobial Activity and Non-toxicity Assessment** We evaluate antimicrobial activity using  
 850 APEX (Wan et al., 2024) predictions for *E. coli* and *S. aureus* providing species-specific MIC predic-  
 851 tions for clinically relevant pathogens. Toxicity assessment is performed using our trained hemolytic  
 852 toxicity classifier as described in A.4.3

853 **Fréchet Biological Distance** To evaluate the quality of generated peptides in biologically relevant  
 854 embedding space, we compute Fréchet Biological Distance (FBD) using fine-tuned ESM2 embed-  
 855 dings. The ESM2-t12 model (Lin et al., 2023) was fine-tuned for binary antimicrobial activity  
 856 classification using active/inactive labels with thresholds of  $\leq 32 \mu\text{g/ml}$  for active and  $\geq 128 \mu\text{g/ml}$   
 857 for inactive peptides.

864  
865  
866  
867  
868  
869  
870  
871  
872  
873  
874  
875  
876

r

Table 3: Model hyperparameters and training details.

Parameter	Value
<b>Architecture</b>	
Attention Heads	4
Transformer Layers	6
Latent Dimension	56
Positional Encoding	Additive
Dropout Rate	0.1
Layer Normalization	Enabled
<b>Training</b>	
Optimizer	Adam
Learning Rate	0.001
Batch Size	512
Epochs	3100
IWAE Samples ( $K$ )	10
<b>VAE Regularization</b>	
$\beta$ Initial	0.00001
$\beta$ Final	0.1
$\beta$ Warmup Steps	8000
<b>Attribute Regularization</b>	
Regularized Dimensions	[0, 1, 2, 3, 4, 5]
$\gamma$ Initial	0.00001
$\gamma$ Final	20
$\gamma$ Warmup Steps	8000
$\gamma$ Triggered epoch	1000
$\delta$	0.1 for PepGlider for physicochemical attributes 0.6 for PepGlider only antimicrobial attributes
<b>Data</b>	
Max Sequence Length	25
Vocabulary Size	20
Property Normalization	Quantile (10 bins)
Properties Regularized	Length, Charge, Hydrophobicity, MIC E.coli, MIC S.aureus, Non-toxicity

907  
908  
909  
910  
911  
912  
913  
914  
915  
916  
917

918 FBD is computed analogously to Fréchet Inception Distance (Heusel et al., 2017) by modeling the  
 919 distributions of ESM2 embeddings as multivariate Gaussians:  
 920

$$921 \quad \text{FBD} = \|\boldsymbol{\mu}_{\text{real}} - \boldsymbol{\mu}_{\text{gen}}\|_2^2 + \text{Tr}(\boldsymbol{\Sigma}_{\text{real}} + \boldsymbol{\Sigma}_{\text{gen}} - 2(\boldsymbol{\Sigma}_{\text{real}}\boldsymbol{\Sigma}_{\text{gen}})^{1/2}) \quad (12)$$

922 where  $\boldsymbol{\mu}$  and  $\boldsymbol{\Sigma}$  represent the mean and covariance of the embedding distributions for real and  
 923 generated peptides, respectively.  
 924

## 925 Sequence Quality Metrics

- 928 • **Validity** measures how well generated peptides conform to the training distribution by  
 929 computing FBD between generated sequences and the training dataset using ESM2 em-  
 930 beddings.
- 931 • **Diversity** is a fraction of unique generated sequences not present in the training dataset.
- 932 • **Novelty** is computed using average pairwise Levenshtein distance among generated se-  
 933 quences.
- 934 • **AMP Potential** evaluates similarity to experimentally validated antimicrobial peptides by  
 935 computing FBD to a curated set of active peptides with documented MIC  $\leq 32 \mu\text{g/ml}$   
 936 against at least one bacterial strain in DBAASP.

938 **Disentanglement Quality Metrics** Following Pati & Lerch (2021), we assess PepGlider’s disen-  
 939 tanglement quality using five established objective metrics:  
 940

- 941 • **Interpretability** measures how well individual latent dimensions align with specific at-  
 942 tributes by evaluating the variance explained by the most informative dimension for each  
 943 attribute:

$$944 \quad \text{Interpretability} = \frac{1}{K} \sum_{k=1}^K \max_j R^2(a_k, z_j) \quad (13)$$

945 where  $K$  is the number of attributes,  $a_k$  is the  $k$ -th attribute, and  $R^2(a_k, z_j)$  is the coeffi-  
 946 cient of determination between attribute  $k$  and latent dimension  $j$ .  
 947

- 948 • **Spearman Correlation Coefficient (SCC)** quantifies the monotonic relationship between  
 949 latent dimensions and target attributes:  
 950

$$951 \quad \text{SCC} = \frac{1}{K} \sum_{k=1}^K \max_j |\rho_s(a_k, z_j)| \quad (14)$$

952 where  $\rho_s$  denotes the Spearman correlation coefficient.  
 953

- 954 • **Modularity** assesses whether each attribute is controlled by a distinct set of latent dimen-  
 955 sions, measuring the degree of separation between attribute-dimension associations.  
 956
- 957 • **Mutual Information Gap (MIG)** evaluates disentanglement by measuring the difference  
 958 between the top two mutual information values:  
 959

$$960 \quad \text{MIG} = \frac{1}{K} \sum_{k=1}^K \frac{I(a_k; z_{j^{(1)}}) - I(a_k; z_{j^{(2)}})}{H(a_k)} \quad (15)$$

961 where  $j^{(1)}$  and  $j^{(2)}$  are the indices of the latent dimensions with highest and second-highest  
 962 mutual information with attribute  $k$ , and  $H(a_k)$  is the entropy of attribute  $k$ .  
 963

- 964 • **Separated Attribute Predictability (SAP)** measures how well attributes can be predicted  
 965 from individual latent dimensions while being unpredictable from others, indicating effec-  
 966 tive separation of attribute control.  
 967

968 Results across all metrics are reported in Table A.5.1.  
 969  
 970

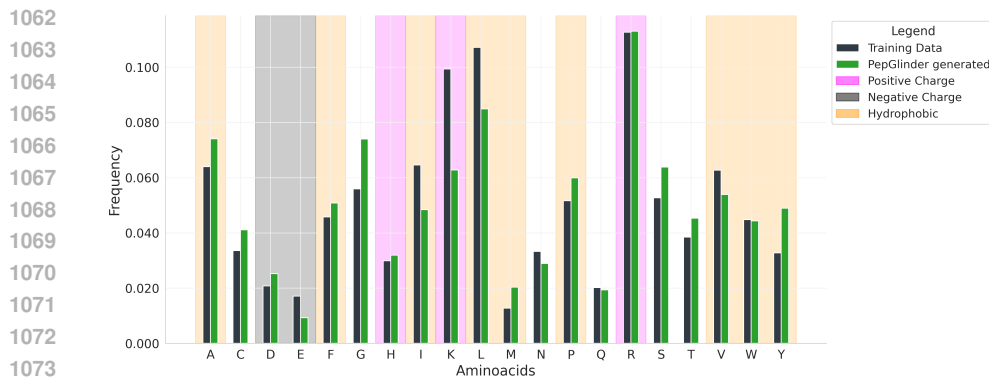
972 A.5 EXTENDED RESULTS  
973  
974975 A.5.1 DISENTANGLEMENT DETAILED ANALYSIS  
976  
977  
978  
979  
980

Model	Attribute	Interpretability ( $\uparrow$ )	SCC ( $\uparrow$ )	Modularity ( $\uparrow$ )	MIG ( $\uparrow$ )	SAP ( $\uparrow$ )
VAE	Length	0.542	0.754	0.893	0.012	0.022
	Charge	0.088	0.320	0.660	0.001	0.026
	Hydrophobicity	0.080	0.309	0.736	0.000	0.009
HydrAMP	Length	0.951	0.973	0.957	0.056	0.020
	Charge	0.024	0.439	0.868	0.003	0.042
	Hydrophobicity	0.178	0.440	0.867	0.000	0.029
Transformer	Length	0.014	0.289	0.799	0.005	0.038
	Charge	0.022	0.333	0.723	0.004	0.013
	Hydrophobicity	0.261	0.494	0.975	0.008	0.121
ARVAE	Length	0.994	0.995	<b>0.999</b>	0.895	0.948
	Charge	0.947	0.994	0.979	0.280	0.655
	Hydrophobicity	0.921	0.996	0.177	0.211	0.621
PepGlider	Length	0.977	0.995	<b>0.999</b>	0.856	0.927
	Charge	0.934	0.991	0.980	0.292	0.649
	Hydrophobicity	0.881	<b>0.998</b>	0.976	0.211	0.587
PepGlider w/o normalization	Length	0.994	0.995	<b>0.999</b>	0.884	0.953
	Charge	0.958	0.992	0.981	0.297	0.670
	Hydrophobicity	0.990	0.997	0.983	0.257	0.690
PepGlider with signum	Length	0.994	0.995	<b>0.999</b>	<b>0.896</b>	0.951
	Charge	0.950	0.994	0.980	0.285	0.655
	Hydrophobicity	0.921	0.996	0.973	0.177	0.612
PepGlider w z-score normalization	Length	<b>0.996</b>	0.995	<b>0.999</b>	0.882	<b>0.959</b>
	Charge	0.966	0.982	0.982	<b>0.321</b>	0.668
	Hydrophobicity	0.937	<b>0.998</b>	0.980	0.231	0.631

999  
1000 Table 4: **Detailed disentanglement quality metrics for PepGlider and baseline and ablation**  
1001 **methods.** Higher scores indicate better disentanglement for all metrics.  
1002  
1003  
1004  
1005  
1006  
1007

Model	Attribute	Interpretability ( $\uparrow$ )	SCC ( $\uparrow$ )	Modularity ( $\uparrow$ )	MIG ( $\uparrow$ )	SAP ( $\uparrow$ )
VAE	MIC <i>E. coli</i>	0.087	0.287	0.815	0.001	0.029
	MIC <i>S. aureus</i>	0.076	0.275	0.795	0.001	0.027
	Nontoxicity	0.054	0.550	0.897	0.002	0.020
HydrAMP	MIC <i>E. coli</i>	0.000	0.295	0.928	0.000	0.020
	MIC <i>S. aureus</i>	0.000	0.248	0.931	0.001	0.012
	Nontoxicity	0.007	0.320	0.931	0.002	0.009
Transformer	MIC <i>E. coli</i>	0.129	0.365	0.945	0.001	0.008
	MIC <i>S. aureus</i>	0.090	0.304	0.932	0.000	0.006
	Nontoxicity	0.039	0.371	0.945	0.001	0.027
PepGlider	MIC <i>E. coli</i>	0.566	0.962	0.992	0.074	0.022
	MIC <i>S. aureus</i>	<b>0.758</b>	0.933	0.991	0.062	<b>0.236</b>
	Nontoxicity	0.332	<b>0.992</b>	<b>0.994</b>	<b>0.075</b>	0.123

1020  
1021 Table 5: **Detailed attribute-specific disentanglement quality metrics results across antimicro-**  
1022 **bial properties (MIC *E. coli*, MIC *S. aureus*, nontoxicity) for PepGlider and baseline methods.**  
1023 Higher scores indicate better disentanglement for all metrics.  
1024  
1025

1026 A.5.2 RECONSTRUCTION  
1027  
1028  
1029  
1030  
1031  
1032  
1033  
1034  
1035  
1036  
1037  
1038  
1039  
1040  
1041  
1042  
1043  
1044  
1045  
1046  
1047  
1048  
1049  
1050  
1051  
1052  
1053  
1054  
1055  
1056  
1057  
1058  
1059  
1060  
1061

1076 Figure 9: **Reconstruction quality assessment for PepGlider-generated peptides.** Amino acid  
1077 frequency distributions comparing generated peptides (green bars) with training data (black bars),  
1078 demonstrating that PepGlider maintains realistic compositional patterns despite attribute regulariza-  
1079 tion constraints. Amino acids crucial for hydrophobicity are highlighted in orange, and amino acids  
contributing to positive charge and negative charge are highlighted in pink and gray, respectively.

1080  
1081

## A.5.3 ABLATIONS

1082

1083

1084

1085

1086

1087

1088

1089

1090

1091

1092

1093

1094

1095

1096

1097

1098

1099

1100

1101

1102

1103

1104

1105

1106

1107

1108

1109

1110

1111

1112

1113

1114

1115

1116

1117

1118

1119

1120

1121

1122

1123

1124

1125

1126

1127

1128

1129

1130

1131

1132

1133

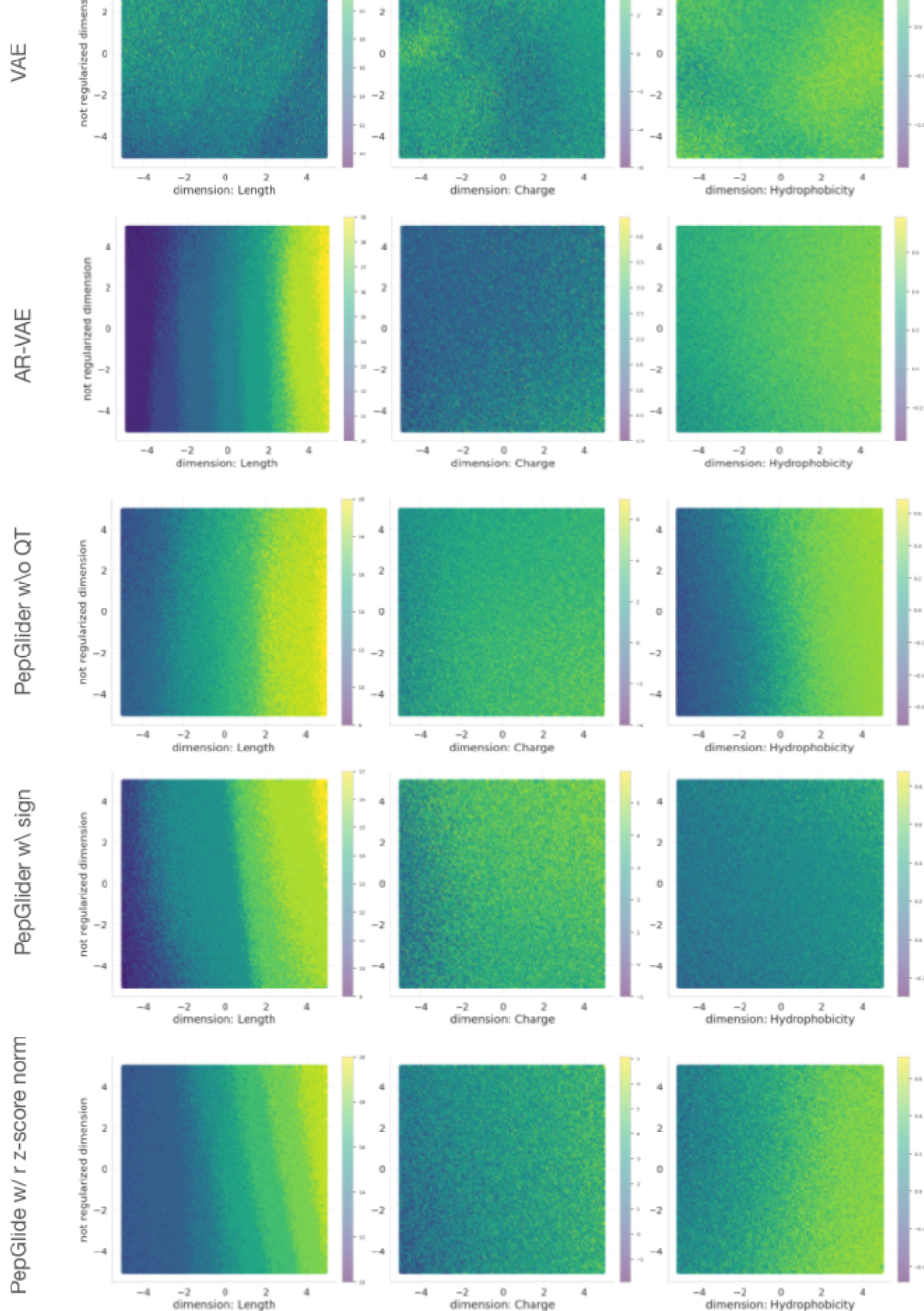


Figure 10: Latent ablations

**Latent visualizations**

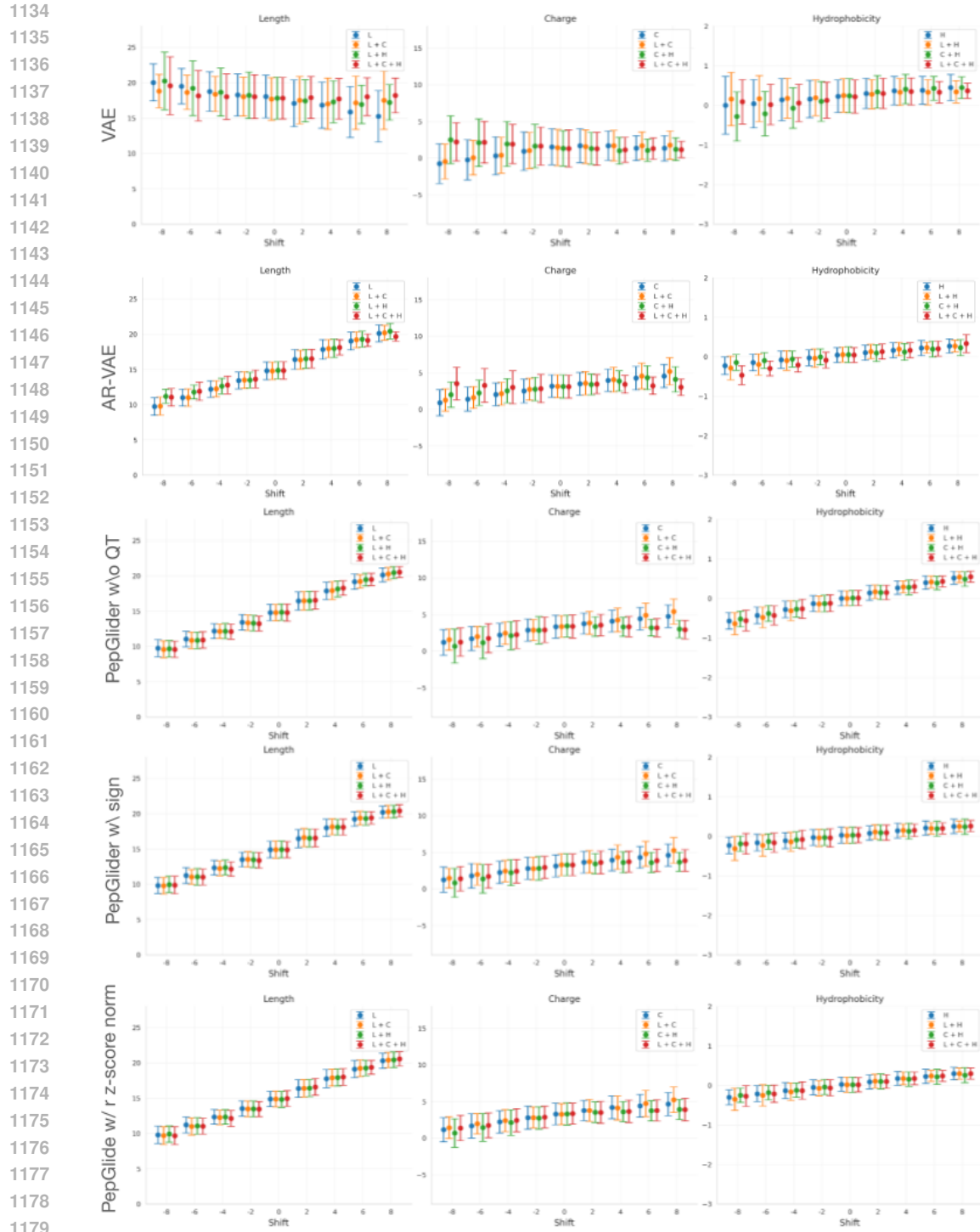


Figure 11: Multiconditioning

## Multiconditioning

